

Excitonic properties of F-centers in α -alumina from First Principles Calculation

Tathagata Biswas and Manish Jain*

*Center for Condensed Matter Theory, Department of Physics,
Indian Institute of Science, Bangalore, 560012*

(Dated: March 29, 2022)

Abstract

We use state-of-the art GW-BSE formalism to study electronic structure and optical properties of oxygen vacancies in α -alumina. Many body perturbation theory within GW approximation in recent years have been used extensively to study excited state properties of a wide range of systems. Moreover, solving Bethe-Salpeter equation (BSE) enable us to capture excitonic effects in a material. We compute the charge transition levels (CTLs) for oxygen vacancies using DFT+GW formalism. We propose an alternative approach to calculate these CTLs, which provides a more efficient way to perform electrostatic correction required because of finite supercell sizes and periodic boundary condition used in first principles calculations. We find that oxygen vacancy in this material has deep donor levels, (+2/+1) at 2.5 eV and a (+1/0) level at 3.8 eV above the VBM. We also study F-center absorption and emission processes using constrained-DFT and BSE. Our calculated absorption and emission energies are in excellent agreement with experimental results.

I. INTRODUCTION

Aluminium oxide with corundum structure (α -alumina) is perhaps one the most used structural ceramic in the world. The application of this material ranges from high-temperature structural ceramics, abrasive, dielectric insulators, catalyst to optical devices¹⁻⁴. α -alumina has been used not only in traditional fields such as cutting tools in industries, substrates for the growth of thin metal, semiconductor, and insulator films but also in exciting new applications such as strong durable optical fibres or scratch resistant screens on mobile electronics devices^{3,4}. This is because of its unusual combination of mechanical, chemical and electronic properties². However, all these properties can alter dramatically as we consider point defects or impurities in an otherwise perfect crystal^{5,6}. For instance anionic vacancy in a crystal which is filled by one or more electrons (F-center or color center) has been found to absorb light in the visible spectrum making a wide band gap transparent material, colored⁷. As a result, not only aluminium oxide as a material but also defects in aluminium oxide have been focus of extensive theoretical and experimental study for past few decades⁷⁻¹². Oxygen related defects especially oxygen vacancies, are known to be a common defect in most oxides¹³. However, the abundance of experimental data available in this field has not been complemented with theoretical studies to provide meaningful insight into these defects.

Thermodynamic CTLs provide useful information from an electronic or optoelectronic application point of view. CTL not only describes whether the defect state is going to act as a donor or acceptor but also reports if it is a shallow one ($\sim k_B T$ from bands edges) or lies deep inside the band gap¹⁴. Shallow levels being close to VBM or CBM can produce electrons in conduction band or holes in valence band though thermal excitation alone and therefore results in controlled n -type or p -type conductivity. However, sometimes shallow levels are not technologically desirable. If unintentional dopants (impurities) introduces a shallow level, it can results in a reduction of doping efficiency. A deep level can also affect device performance and may reduce device lifetimes of electronic or optoelectronic devices. As it can provide uncontrolled radiative or nonradiative recombination channels. It should be noted that in recent years, deep levels have been used constructively as well. For example, one can use them to pin the Fermi level in an energy region far from the band edges^{15,16}. Moreover, deep levels have also been used as single spin centers for quantum computing in

systems like nitrogen-vacancy (NV) center in diamond¹⁷.

II. COMPUTATIONAL METHODS

We perform all the DFT calculations using generalized gradient approximation (GGA)¹⁸ and norm-conserving pseudopotentials¹⁹ as implemented in the QUANTUM ESPRESSO package²⁰. The wavefunctions are expanded in plane waves with energy upto 75 Ry. The calculations for perfect crystal have been done using a unit cell containing 30 atoms, with a $4\times 4\times 2$ k-point sampling of the Brillouin zone. For the calculations with oxygen vacancies in various charge states, we use $2\times 2\times 1$ and $3\times 3\times 1$ supercells, containing 120 and 270 atoms respectively, to exclude any short range defect-defect interactions. The Brillouin zone for $2\times 2\times 1$ and $3\times 3\times 1$ supercells, was sampled using $2\times 2\times 2$ and Γ -point respectively. We simulate different charge states ($q = 0, 1, 2$) of the oxygen vacancy.

Quasiparticle and optical properties are calculated within the GW-BSE formalism as implemented in the BerkeleyGW package²¹. To compute the quasiparticle energies (E^{QP}) we solve the Dyson equation²², where the self energy operator ($\Sigma(E)$) has been calculated within G_0W_0 approximation. The dielectric matrix (ϵ) is calculated within the random phase approximation (RPA) and expressed in a plane-wave basis with plane wave energies upto 25 Ry. The matrix is calculated at zero frequency and extended to finite frequencies using generalized plasmon pole model proposed by Hybertsen and Louie²³. In case of 30 atom unit cell, we include 1000 bands while performing sum over unoccupied states involved in the dielectric matrix and self-energy calculations. For $2\times 2\times 1$ and $3\times 3\times 1$ supercells, we increase the number of bands to 4000 and 9000 respectively. To study electron-hole interaction and excitonic effects we solve the Bethe-Salpeter equation²⁴. Electron-hole interaction kernel for BSE calculation is computed with 44 valence and 11 conduction bands. The calculated kernel is extrapolated from a $4\times 4\times 2$ to a finer $10\times 10\times 5$ k-point sampling of the Brillouin zone. These parameters are sufficient to obtain a converged optical spectrum for energies upto ~ 5 eV from absorption edge.

The formation energy of a point defect, $E_q^f(\mathbf{R})[\epsilon_F]$, in charge state q , with all the atoms at coordinates $\{\mathbf{R}\}$ and the chemical potential of the electron (Fermi level) ϵ_F , can be defined as¹⁴,

$$E_q^f(\mathbf{R})[\epsilon_F] = E_q^{\text{def}}(\mathbf{R}) - [E^{\text{perf}} + \sum_i n_i \mu_i] + [\epsilon_F + E_v]q \quad (1)$$

where $E_q^{\text{def}}(\mathbf{R})$ is the total energy of the defect supercell in charge state q with all the atoms at coordinates $\{\mathbf{R}\}$ and E^{perf} is the total energy of the perfect supercell (without any defects). n_i refers to the number of atoms removed ($n_i < 0$) from or added to ($n_i > 0$) the perfect supercell to make the defect supercell. The removed/added atoms are exchanged from a bath with chemical potential μ_i . It should be noted that we have defined ϵ_F with respect to valence band maxima (E_v).

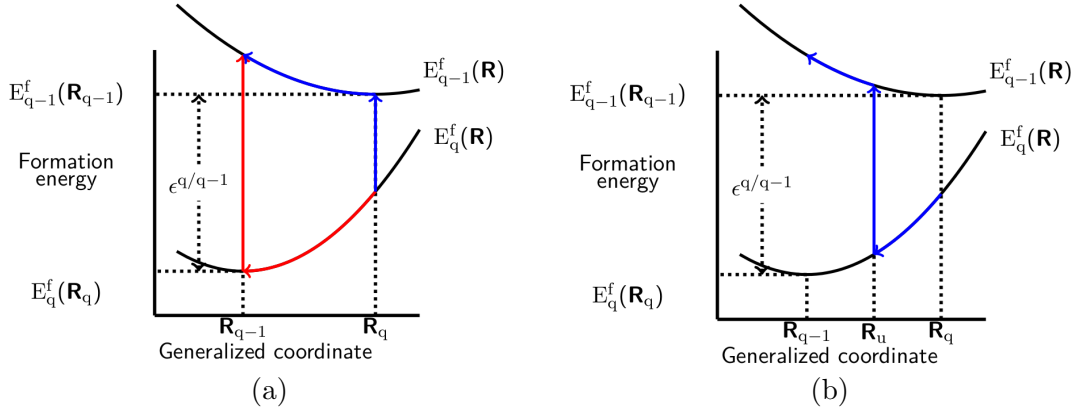


FIG. 1. Paths that can take the system being at equilibrium with defect at charge state q to one where it is at charge state $q - 1$. Paths that is equivalent to using (a) Eq. 3 (red) Eq. 4 (blue) and (b) Eq. 5 have been shown.

Thermodynamic charge transition level (CTL) $\epsilon^{q/q-1}$, is defined as the value of the electron chemical potential (ϵ_F) at which the charge state of the defect changes from q to $q - 1$. It can be written in terms of formation energies as¹⁴,

$$\epsilon^{q/q-1} = E_{q-1}^f(\mathbf{R}_{q-1})[\epsilon_F = 0] - E_q^f(\mathbf{R}_q)[\epsilon_F = 0] \quad (2)$$

where $\{\mathbf{R}_q\}$ and $\{\mathbf{R}_{q-1}\}$ denote the equilibrium structures with defect in charge states q and $q - 1$ respectively.

Within standard DFT, one can obtain the formation energies in equilibrium configurations of respective charge states and thus calculate $\epsilon^{q/q-1}$. However, as we have mentioned

earlier that DFT is a theory for ground state properties. Calculating CTL involves addition or removal of one or multiple electrons, therefore can not be accomplished with DFT formalism alone. To overcome this problem we have used a more sophisticated DFT+GW formalism²⁵⁻²⁷. In this method we write the CTL as,

$$\begin{aligned}\epsilon^{q/q-1} &= [E_{q-1}^f(\mathbf{R}_{q-1}) - E_{q-1}^f(\mathbf{R}_q)] + [E_{q-1}^f(\mathbf{R}_q) - E_q^f(\mathbf{R}_q)] \\ &\equiv E_{q-1}^{\text{relax}}[\mathbf{R}_q] + E^{\text{QP}}(\mathbf{R}_q)\end{aligned}\quad (3)$$

The first term ($E_{q-1}^{\text{relax}}[\mathbf{R}_q]$) on the right hand side of Eq. 3 is a relaxation energy. For a system containing a defect in charge state $q - 1$, $E_{q-1}^{\text{relax}}[\mathbf{R}_q]$ is the total energy difference between a structure with all the atoms at coordinates $\{\mathbf{R}_q\}$ and the equilibrium structure (in this case $\{\mathbf{R}_{q-1}\}$). The relaxation energy can be computed accurately within DFT. The second term on the right hand side $E^{\text{QP}}(\mathbf{R}_q)$ of Eqn. 3, involves a change in the electron number as the defect charge changes from q to $q - 1$. This is the electron affinity (EA) of the system containing a defect in charge state q with all the atoms at $\{\mathbf{R}_q\}$. This quasiparticle energy can be computed accurately using the GW formalism. Alternatively, we can write,

$$\begin{aligned}\epsilon^{q/q-1} &= [E_{q-1}^f(\mathbf{R}_{q-1}) - E_q^f(\mathbf{R}_{q-1})] + [E_q^f(\mathbf{R}_{q-1}) - E_q^f(\mathbf{R}_q)] \\ &\equiv E^{\text{QP}}(\mathbf{R}_{q-1}) - E_q^{\text{relax}}[\mathbf{R}_{q-1}]\end{aligned}\quad (4)$$

where $E_q^{\text{relax}}[\mathbf{R}_{q-1}]$ is defined in the same way as $E_{q-1}^{\text{relax}}[\mathbf{R}_q]$ in Eq. 3 and $E^{\text{QP}}(\mathbf{R}_{q-1})$ is the ionization potential (IP) of the system containing a defect in charge state $q - 1$ with all the atoms at $\{\mathbf{R}_{q-1}\}$. In Fig 1(a) we show two paths that can take the system being at equilibrium with defect at charge state q to one where it is at equilibrium with charge state $q - 1$. Using Eq. 3 or Eq. 4 to compute $\epsilon^{q/q-1}$ is equivalent to taking the red or the blue path shown in Fig. 1(a). Following either of the two paths one should get the same Thermodynamic CTLs. This DFT+GW formalism should eliminate the errors in calculating CTLs within standard DFT.

First principles calculations on defects often use periodic boundary condition (PBC) with a finite supercell size. While the supercell can be made to be large enough to eliminate any short range interaction between a defect and its periodic image, the long range interactions, such as Coulomb interaction between charged defects, can not be eliminated entirely. To

tackle this issue, we break down the defect-defect interaction within PBC into a short-range part such as quantum-mechanical (overlap of the wave functions), and a long range part such as elastic or electrostatic interactions. In practice, we work with a supercell size that is large enough to eliminate any short-range defect-defect interactions. For the long-range electrostatic and elastic interactions we use a correction/extrapolation scheme. As elastic interactions decay faster ($1/L^3$) than electrostatic interactions ($1/L$), typically, one worries more about the later. In this study, we use FNV electrostatic correction scheme²⁸ as implemented in CoFFEE package²⁹.

While calculating relaxation energies using DFT formalism one may be tempted to assume that the electrostatic correction involved is zero as the total energy corrections for two formation energies with defect in the same charge state cancel each other. This is not entirely true, as the lattice screening in case of the two structures are different. The lattice relaxation in the two structures are as if they are screening different defect charges (as they corresponds to $\{\mathbf{R}_q\}$ and $\{\mathbf{R}_{q-1}\}$). Moreover the choice of dielectric constant, while performing eigenvalue correction to compute quasiparticle excitation energies for charged defects is ambiguous if one uses Eq. 3 or Eq. 4. This is because an unknown fraction of lattice dielectric constant is included owing to small supercell sizes. Using either the electronic dielectric constant (ϵ_{elec}) or the full dielectric constant (ϵ_{total}) is not expected to provide accurate electrostatic correction. We propose an alternative path to calculate CTLs which does not suffer from this issue. The CTL can be calculated using the path shown in Fig. 1(b). The CTL using this path can be written as:

$$\begin{aligned} \epsilon^{q/q-1} &= [E_{q-1}^f(\mathbf{R}_{q-1}) - E_{q-1}^f(\mathbf{R}_u)] + [E_{q-1}^f(\mathbf{R}_u) - E_q^f(\mathbf{R}_u)] + [E_q^f(\mathbf{R}_u) - E_q^f(\mathbf{R}_q)] \\ &= E_{q-1}^{relax}[\mathbf{R}_u] + E_u^{QP} - E_q^{relax}[\mathbf{R}_u] \end{aligned} \quad (5)$$

where $\{\mathbf{R}_u\}$ denotes the unrelaxed structure, which can be obtained by removing an atom from perfect supercell without changing positions of any other atoms. We compute $E_q^{relax}[\mathbf{R}_u]$ ($E_{q-1}^{relax}[\mathbf{R}_u]$) using DFT. These relaxation energies correspond to the relaxation of defect supercell with the charge state q or $q - 1$ from $\{\mathbf{R}_u\}$ to corresponding equilibrium structures. Quasiparticle excitation energy in Eq. 5 (E_u^{QP}) can be computed as either IP of the unrelaxed system with defect charge state $q - 1$ (P1) or EA of the same structure with defect charge state q (P2). The choice of path shown in Fig. 1(b) is motivated by the

fact that the dielectric constant required for electrostatic correction of the E_u^{QP} term is well defined (ϵ_{elec}).

To relax the structure for the triplet excited state of F-center we use constrained-DFT calculation. We perform a spin polarized DFT calculation and fix the occupations in such a way that one electron from defect state gets promoted to the conduction band with its spin flipped. Therefore the system remains neutral and mimics a triplet excited state. We show that using this method we can calculate relaxation energies of triplet excited state, which combined with BSE calculation provide very good agreement with experimental photoluminescence emission results. We find that the geometries obtained within such a relaxation is very close to the F^+ geometry.

III. RESULTS AND DISCUSSION

α -alumina has a hexagonal unit cell (space group $R\bar{3}C$) containing 30 atoms or 6 formula units. It can also be constructed with a smaller rhombohedral unit cell containing 10 atoms (2 formula units). We have used hexagonal unit cell of α -alumina in all our calculations.

parameters	this work (LDA)	this work (GGA)	Ref. ¹¹ (LDA)	Ref. ⁸ (GGA)	Expt. ³⁰
a in Å	4.68	4.81	4.69	4.82	4.76
c in Å	12.45	13.13	12.79	13.16	12.99
E_g in eV	6.75	5.82	6.72	5.82	9.4

TABLE I. Comparison between lattice parameters and band gap values from our calculations with literature

The lattice parameters of α -alumina that we found in our calculation are in very good agreement with previous DFT calculations^{8,11} and experimental values³⁰ as shown in Table. I. Our calculations show that the band gap of this material has a strong lattice parameter dependence. We study the band gap of α -alumina as we change the in-plane lattice parameter (a) by keeping the c/a ratio fixed using both LDA (PZ) and GGA (PBE) and show the results in Fig. 2. The band gap of this material increases almost linearly as we decrease the in-plane lattice parameter (a). Due to overbinding effect of LDA, the band gap of the

equilibrium structure within LDA is overestimated compared to that found within GGA (using its equilibrium structure). As we can see in Fig. 2 the difference between GGA and LDA band gap value at their respective equilibrium lattice parameter is ~ 1 eV. This difference is almost entirely because of the difference in the lattice parameters in these two calculations. These results explain the large variation in the values of band gap reported in literature⁸⁻¹¹. Fig. 2 also shows our calculation of the GW quasiparticle gap starting from a DFT calculation with GGA. The GW gap also varies significantly as a function of in-plane lattice parameter inheriting the dependence from the DFT starting point.

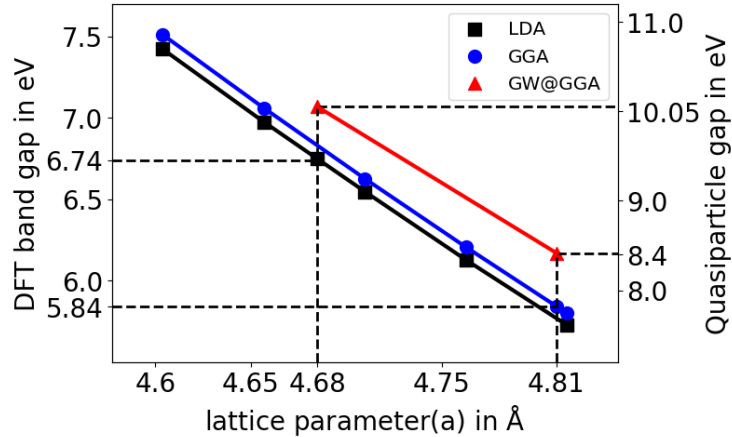


FIG. 2. Variation of band gap with lattice parameter a calculated using both GGA and LDA, the equilibrium lattice parameter in both case and the corresponding band gap has been marked. In these calculations the c/a ratio was fixed to the equilibrium value.

Results (in eV)	this work	Reference ¹¹	Expt. ¹⁰ at 0K	Expt. ¹⁰ at 300K
E_g	9.1	9.36	9.57	9.31
E_{EBE}	0.37	0.4	0.13	0.15

TABLE II. Quasiparticle band gap and exciton binding energy obtained from our calculation compared with values reported in literature

Table. II shows the quasiparticle band gap (E_g) and exciton binding energy (E_{EBE}) ob-

tained from our calculation and compares them with values reported in the literature. Our calculated quasiparticle band gap is in reasonable agreement with previous GW calculations done on this material¹¹. The difference between the two calculations can be attributed to the difference in the lattice parameters used. Previous study¹¹ used lattice parameter values obtained from DFT calculation using LDA, which is expected to result in a larger DFT as well as quasiparticle gap compared to one obtained using experimental lattice parameters as we have shown earlier (Fig. 2). However, the exciton binding energy reported in that¹¹ study is very close to the one we obtain with using experimental lattice parameters. This suggests a weaker lattice parameter dependence of E_{EBE} compared to E_g . We also find that GW quasiparticle gap using experimental lattice constants (9.1 eV) is in close agreement with the experimental gap at room temperature (9.31 eV)¹⁰. This is because we have used we have used the experimental lattice parameters obtained at room temperature in our studies³⁰.

Fig. 3 shows the defect levels inside the band gap originated due to an oxygen vacancy, calculated from DFT as well GW calculations performed on a $3 \times 3 \times 1$ supercell. We show the position as well occupation of these levels for three possible charge states, neutral (V_{O}^0) +1 (V_{O}^{+1}), +2 (V_{O}^{+2}). For V_{O}^0 we find one doubly occupied spin degenerate level inside the gap. As we remove one electron from the neutral defect the system becomes spin polarized with only one of the spin-split defect level occupied. Removing one more electron from the defect results in an unoccupied spin degenerate level inside the gap. The defect levels obtained from DFT calculations do not move rigidly as we include quasiparticle corrections. The occupied defect levels move higher in energy by only ~ 0.3 eV, whereas the unoccupied levels move by 2.1 eV and 2.6 eV for V_{O}^{+1} and V_{O}^{+2} respectively. In the +2 and +1 charge state the four Al atoms next to oxygen vacancy on an average relax outward by ~ 0.23 Å and ~ 0.1 Å respectively, whereas in the neutral charge state, the Al atoms relax inward by ~ 0.05 Å.

In Table. II we show thermodynamic charge transition levels calculated using Eq. 3 (P1) and Eq. 4 (P2) with two different cell sizes, $2 \times 2 \times 1$ and $3 \times 3 \times 1$. We report the values obtained with (ec) as well as without electrostatic corrections (we) to show the importance of electrostatic correction while calculating CTL. We have used $\epsilon = \epsilon_{\text{elec}} = 3.1$ while performing the electrostatic corrections, which we have taken from the literature³¹. One can see from Table. II the CTL calculated without electrostatic correction following P1 and P2

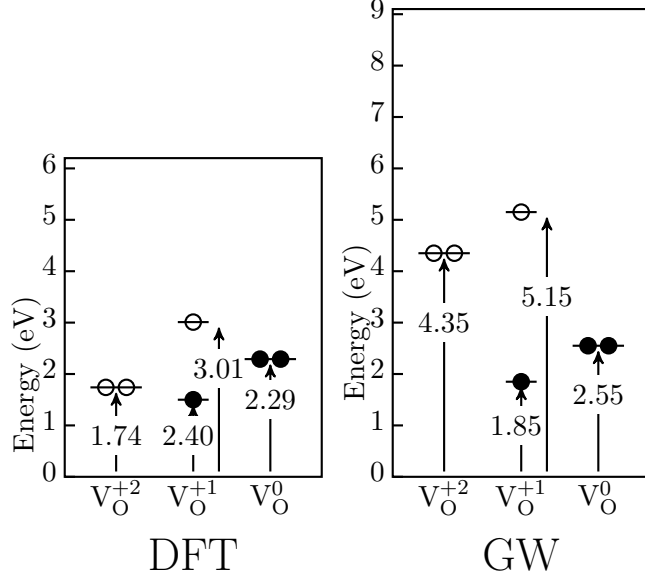


FIG. 3. Defect level positions and their occupations for different charge states from DFT as well as GW calculation

CT levels	P1 ^{we}	P2 ^{we}	Δ^{we}	P1 ^{ec}	P2 ^{ec}	Δ^{ec}	Mean ^{ec}
$\epsilon_{120}^{+1/0}$	4.87	3.58	1.3	3.66	3.58	0.08	3.62
$\epsilon_{270}^{+1/0}$	4.86	3.77	1.09	3.96	3.77	0.19	3.86
$\epsilon_{120}^{+2/+1}$	5.14	3.72	1.42	2.79	2.51	0.28	2.65
$\epsilon_{270}^{+2/+1}$	5.04	3.84	1.20	3.23	2.94	0.29	3.08

TABLE III. Charge transition levels calculated with two different cell sizes using Eq. 3 (P1) and Eq. 4 (P2). We report the values obtained with (ec) or without electrostatic corrections (we) and the differences between them (Δ).

are different by ~ 1 eV (Δ^{we})²⁵. These values should be the same as the CTL is a thermodynamic quantity and should not depend on the path we chose to calculate it. Once we include the electrostatic correction to the E^{QP} values involving a charged defect calculation we can see the Δ values decrease dramatically²⁵. However we find that the Δ values with including electrostatic correction are still large and the CTL has significant cell size dependence. The remaining discrepancy is due to the choice of dielectric constants used in the electrostatic corrections. The electrostatic correction performed here are calculated using ϵ_{elec} . As discussed previously, by using ϵ_{elec} we assume the charges localized at defect

sites are interacting through electronically screened Coulomb interaction only and lattice screening (ϵ_{latt}) does not play any role. But during the process of structural relaxation the surrounding atoms move to screen the defect charges. Therefore, in any finite supercell size we have some lattice screening effects. Moreover we are assuming there is no electrostatic corrections required for E^{relax} , which we show, in the following section, is not necessarily the case.

CT levels	E_{q-1}^{relax}	E_q^{relax}	E_{P1}^{QP}	$\epsilon^{q/q-1}$	E_{P2}^{QP}	$\epsilon^{q/q-1}$	Δ	Mean
$\epsilon^{+1/0}$	-0.12	-1.09	2.87	3.84	2.94	3.9	0.07	3.87
$\epsilon^{+2/+1}$	-1.09	-3.79	-0.14	2.56	-0.09	2.61	0.05	2.58

TABLE IV. Charge transition levels calculated with $3\times 3\times 1$ supercell using Eq. 5 with including electrostatic corrections for both E^{QP} and E^{relax}

To address the issues mentioned earlier and to eliminate the remaining error in CTLs following P1 and P2 we calculate the CTLs using Eq. 5. In these calculation the quasiparticle transition energies are calculate at the unrelaxed structures. As a result one can use ϵ_{elec} to perform electrostatic corrections for E^{QP} . While in principle one can construct an electrostatic model for the correction to E^{relax} , we have computed it by extrapolating the relaxation energies from 4 supercell sizes. The E^{relax} value extrapolated to infinite system size is used to correct the E^{relax} for the finite cell sizes. In Table. IV we show charge transition levels calculated with $3\times 3\times 1$ supercell using Eq. 5 using IP (P1) as well as EA (P2) values of unrelaxed system with defect at respective charge states. We have performed the electrostatic corrections for E^{QP} using FNV scheme. We find that the Δ values are now less than 0.1 eV. Moreover in Table. V we show that the CTL values calculated in this way has a much smaller cell size dependence (< 0.15 eV). Calculating CTL using Eq. 5 provides a very efficient way to perform electrostatic corrections and to obtain more accurate results than using Eq. 3 or Eq. 4.

With modified DFT+GW formalism our calculation shows that the oxygen vacancy has two donor levels within the gap of α -alumina. It has a transition level (+2/+1) at 2.5 eV and a (+1/0) level at 3.8 eV above the VBM.

The optical absorption of F-center in α -alumina involves excitation from 1S -like ground state to a singlet excited state, $^1P^{7,32}$. The system then relaxes to a triplet excited state

Cell size	2×2×1	3×3×1	Δ	Mean
$\epsilon^{+1/0}$	3.77	3.9	0.13	3.83
$\epsilon^{+2/+1}$	2.42	2.56	0.14	2.49

TABLE V. Charge transition levels calculated with 2×2×1 and 3×3×1 supercell using Eq. 5 with including electrostatic corrections for both E^{QP} and E^{relax}

(3P) using a non-radiative relaxation process. The emission occurs when the system goes through a $^3P \rightarrow ^1S$ transition. As this is a spin-forbidden transition the lifetime of this process is very high (~ 36 msec)³² and results in photoluminescence. Experimental studies of the F-center in alumina have found the absorption and emission peaks at 6.1 eV and 3 eV respectively.

To study F-center optical absorption we start from the neutral defect supercell. As discussed earlier the ground state in this case has a doubly occupied defect state at 2.55 eV from the VBM (Fig. 3). To study the singlet transition ($^1S \rightarrow ^1P$) we perform a BSE calculation including both the direct (K^d) and exchange (K^x) contributions in the electron-hole interaction kernel. We find the lowest energy exciton at 6.2 eV. This agrees very well with the experimental absorption peak at 6.1 eV³². Without electron-hole interaction this absorption peak would have been at 6.55 eV, indicating a strong excitonic effect with a exciton binding energy of ~ 0.35 eV. This exciton binding energy is very close to the bulk α -alumina value (0.37 eV).

If the absorption ($^1S \rightarrow ^3P$) and emission ($^3P \rightarrow ^1S$) energies are denoted by E_{ab} and E_{em} respectively. It is evident that they are related as,

$$\begin{aligned}
E_{ab} &= E_{em} + (E^{3P}[R_{1S}] - E^{3P}[R_{3P}]) + (E^{1S}[R_{3P}] - E^{1S}[R_{1S}]) \\
&= E_{em} + E_{relax}^{3P} + E_{relax}^{1S}
\end{aligned}
\tag{6}$$

where E_{relax}^{3P} is the triplet excited state relaxation energy and E_{relax}^{1S} is the ground state relaxation energy. The E_{relax}^{3P} is the total energy difference, when the system is in triplet excited state, between all the atoms at the 1S equilibrium structure ($\{\mathbf{R}_{1S}\}$) and it's own equilibrium structure. Similarly, E_{relax}^{1S} is the the total energy difference, when the system is in singlet ground state, between all the atoms at the 1S equilibrium structure ($\{\mathbf{R}_{3P}\}$) and it's own equilibrium structure.

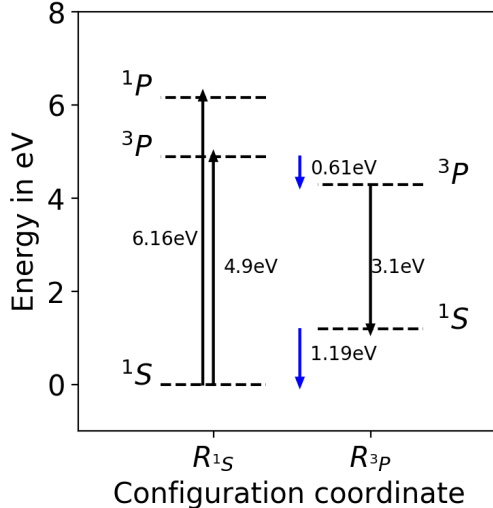


FIG. 4. Energy-level scheme for absorption and emission processes associated with F-center in α -alumina

The emission process involves ${}^3P \rightarrow {}^1S$ transition. To study this process we calculated the “dark” triplet solution of the BSE with the system at the equilibrium structure of the ground state. Within BSE, triplet solutions are found by making the exchange contribution (K^x) in the electron-hole kernel to be zero. We found that the lowest energy required for this transition is at 4.9 eV. This energy can be interpreted as E_{ab} in Eqn. 6. We then calculate excited state relaxation energy (E_{relax}^{3P}) using constrained-DFT as discussed earlier and we find it to be 0.61 eV. The ground state relaxation energy (E_{relax}^{1S}) is then computed by finding the excited state equilibrium structure (R_{3P}) from constrained-DFT calculation. We find this value to be 1.18 eV. Using these results in Eqn. 6 we find that the emission process should be at 3.1 eV. This is in excellent agreement with the experimental photoluminescence emission peak³². In Fig 4 we explain the absorption and emission process and also show all the excitation and relaxation energies calculated for absorption and emission of F-center in α -alumina.

IV. CONCLUSION

We have used first-principles methods to study electronic and optical properties of α -alumina. Using DFT+GW formalism we calculate the thermodynamic charge transition levels for oxygen vacancies in this material. We propose a modified version of this formalism

which can be used to perform electrostatic correction more efficiently and therefore provide more accurate CTL values. We find that oxygen vacancy in this material has deep donor levels, (+2/+1) at 2.5 eV and a (+1/0) level at 3.8 eV above the VBM. We also study the optical absorption and emission process of neutral oxygen vacancy in α -alumina (F-center) using GW-BSE methodology. For the photoluminescence emission process, we use constrained-DFT to simulate ground and excited state relaxation processes. Our calculation suggests that F-center in this material will have absorption and emission peak near 6.2 eV and 3.1 eV respectively, which is in very good agreement with experimental results.

* mjain@iisc.ac.in

- ¹ M. J. Pearson, *Industrial & Engineering Chemistry Product Research and Development* **16**, 154 (1977).
- ² P. Auerkari, *Mechanical and physical properties of engineering alumina ceramics* (Technical Research Centre of Finland Espoo, 1996).
- ³ P. Dragic, T. Hawkins, P. Foy, S. Morris, and J. Ballato, *Nature Photonics* **6**, 627 (2012).
- ⁴ J. M. Zahler and C. J. Petti, “Mobile electronic device comprising an ultrathin sapphire cover plate,” (2016), uS Patent 9,369,553.
- ⁵ A. Heuer, N. J. Tighe, and R. Cannon, *Journal of the American Ceramic Society* **63**, 53 (1980).
- ⁶ R. Cannon, W. H. Rhodes, and A. Heuer, *Journal of the American Ceramic Society* **63**, 46 (1980).
- ⁷ B. Evans, *Journal of Applied Physics* **70**, 3995 (1991).
- ⁸ K. Matsunaga, T. Tanaka, T. Yamamoto, and Y. Ikuhara, *Physical Review B* **68**, 085110 (2003).
- ⁹ R. H. French, *Journal of the American Ceramic Society* **73**, 477 (1990).
- ¹⁰ R. H. French, D. J. Jones, and S. Loughin, *Journal of the American Ceramic Society* **77**, 412 (1994).
- ¹¹ A. Marinopoulos and M. Grüning, *Physical Review B* **83**, 195129 (2011).
- ¹² M. Choi, A. Janotti, and C. G. Van de Walle, *Journal of Applied Physics* **113**, 044501 (2013).
- ¹³ C. T. Campbell and C. H. Peden, *Science* **309**, 713 (2005).

- ¹⁴ C. Freysoldt, B. Grabowski, T. Hickel, J. Neugebauer, G. Kresse, A. Janotti, and C. G. Van de Walle, *Reviews of Modern Physics* **86**, 253 (2014).
- ¹⁵ J. Robertson, O. Sharia, and A. Demkov, *Applied Physics Letters* **91**, 132912 (2007).
- ¹⁶ D. Chadi, P. Citrin, C. Park, D. Adler, M. Marcus, and H.-J. Gossmann, *Physical Review Letters* **79**, 4834 (1997).
- ¹⁷ J. Weber, W. Koehl, J. Varley, A. Janotti, B. Buckley, C. Van de Walle, and D. D. Awschalom, *Proceedings of the National Academy of Sciences* **107**, 8513 (2010).
- ¹⁸ J. P. Perdew, K. Burke, and M. Ernzerhof, *Physical Review Letters* **77**, 3865 (1996).
- ¹⁹ N. Troullier and J. L. Martins, *Physical Review B* **43**, 1993 (1991).
- ²⁰ P. Giannozzi, S. Baroni, N. Bonini, M. Calandra, R. Car, C. Cavazzoni, D. Ceresoli, G. L. Chiarotti, M. Cococcioni, I. Dabo, *et al.*, *Journal of Physics: Condensed Matter* **21**, 395502 (2009).
- ²¹ J. Deslippe, G. Samsonidze, D. A. Strubbe, M. Jain, M. L. Cohen, and S. G. Louie, *Computer Physics Communications* **183**, 1269 (2012).
- ²² L. Hedin and S. Lundqvist, *Solid State Physics* **23**, 1 (1970).
- ²³ M. S. Hybertsen and S. G. Louie, *Physical Review B* **34**, 5390 (1986).
- ²⁴ M. Rohlffing and S. G. Louie, *Physical Review B* **62**, 4927 (2000).
- ²⁵ M. Jain, J. R. Chelikowsky, and S. G. Louie, *Physical Review Letters* **107**, 216803 (2011).
- ²⁶ P. Rinke, A. Janotti, M. Scheffler, and C. G. Van de Walle, *Physical Review Letters* **102**, 026402 (2009).
- ²⁷ M. Hedström, A. Schindlmayr, G. Schwarz, and M. Scheffler, *Phys. Rev. Lett.* **97**, 226401 (2006).
- ²⁸ C. Freysoldt, J. Neugebauer, and C. G. Van de Walle, *Physical Review Letters* **102**, 016402 (2009).
- ²⁹ M. H. Naik and M. Jain, *Computer Physics Communications* **226**, 114 (2018).
- ³⁰ W. Lee and K. Lagerlof, *Journal of Electron Microscopy Technique* **2**, 247 (1985).
- ³¹ Y. Kumagai and F. Oba, *Physical Review B* **89**, 195205 (2014).
- ³² K.-H. Lee and J. Crawford Jr, *Physical Review B* **19**, 3217 (1979).